Sensors & Diagnostics

PAPER

View Article Online
View Journal | View Issue

Cite this: *Sens. Diagn.*, 2024, **3**, 87

Turn-off fluorescence of imidazole-based sensor probe for mercury ions†

Uma Krishnan,[a] Saravanakumar Manickam[b] and Sathiyanarayanan Kulathu Iyer *[a]

Received 11th June 2023,
Accepted 16th October 2023

DOI: 10.1039/d3sd00146f

rsc.li/sensors

A new highly selective and sensitive fluorescent probe, **5** (2-(4-(1,3-dithian-2-yl)phenyl)-4,5-diphenyl-1*H*-imidazole), was developed for Hg^{2+} ion with colorimetric and fluorimetric behavior in organic semi-aqueous solutions. A significant color change from strong cyan blue to weak blue can be observed with probe **5** in association with Hg^{2+}-promoted deprotection of thioacetals. Fluorescent probe **5** can detect quite low levels (5.3 nM) of Hg^{2+} ions. However, we carried out an NMR titration experiment and DFT analysis to characterize the sensor probe **5** with Hg^{2+} ion based on the intramolecular charge transfer mechanism. Furthermore, sensor probe **5** responded quickly across a wide pH range. Most importantly, it could be utilized for excellent selective detection and bio-imaging of Hg^{2+} ion in the *E. coli* cells, as well as Whatman filter paper-based test strips.

1. Introduction

Recognition of mercury, a highly toxic heavy metal pollutant widely distributed in agriculture and industrial water and soil, is essential. Heavy metal ions have received significant attention in supramolecular chemistry due to their notable importance in biological, organic, and ecological assays.[1] At low concentrations, mercury vapor can cause a variety of diseases in the digestive system, as well as Minamata disease, kidney damage, and serious mental and neurological complications, due to their ease of passage through biological membranes.[2] Mercury ion is conventionally used in a wide range of industries, such as coal and gold mining, oil refining, and caustic soda manufacturing.[3] Therefore, it is very important to detect mercury ion levels in both biological and environmental models.[4] Chemical analyses have been used for the determination of toxic heavy metals, for example, atomic absorption spectrometry,[5] mass spectrometry,[6] liquid chromatography,[7] ion chromatography,[8] gas chromatography,[9] HPLC (high-performance liquid chromatography), and X-ray fluorescence spectrometry,[10] as well as fluorescent probe technique. Among these detection methods, the fluorescent probe emission technique is widely accepted due to its on-site high-sensitivity detection with fast response, low cost, and analysis of real samples. Moreover, the multistep syntheses often require the protection of functional groups, which then have to be deprotected for selective detection on a particular site.[11] A typical change accompanying the functional groups results in a distinct change in the electrical and photophysical state of the molecule. Amongst the various aldehyde protective groups, multistep synthesis in cyclic or acyclic thioacetals is frequently engaged, as they are stable in all conditions containing acidic and alkaline media. Furthermore, signaling mechanisms that commonly arise in fluorescent probes are intramolecular charge transfer (ICT),[12–17] photo-induced electron transfer (PET),[18] fluorescence resonance energy transfer (FRET),[19] which are ascribed in the direction of energy/electron transfer using protection/ deprotection approach. Many fluorometric sensor moieties are available for the detection of mercury but with limitations, for example, pyridine and pyrene molecules are very difficult to synthesize and are less sensitive and less specific.[20–23] The turn-off fluorescent chemosensors have been used for mercury-ion sensing in aqueous solutions through intramolecular charge transfer emissions.[24] Pyrene carboxaldehyde-based turn-on chemodosimeter has been reported for the detection of Hg^{2+} by DarShak R. Trivedi *et al.* They have also discussed toxic forms of organic mercury and As^{3+}.[25,26] 2-Aminopyridine derivative-based turn-off fluorescence sensing with selective determination of Hg^{2+} and Fe^{3+} was reported by Subrata Ghosh *et al.*[27] The development of simple fluorometric biosensors and impedimetric chemosensors for the determination of Hg^{2+} ions was reported by D. Tang *et al.*[28–31] A novel coumarin-based absorbance and fluorescence detection of mercury and cyanide ions in aqueous solution were

[a] *Department of Chemistry, School of Advanced Sciences, Vellore Institute of Technology, Vellore-632014, Tamil Nadu, India.*
E-mail: sathiya_kuna@hotmail.com
[b] *Department of Materials Science and Engineering, Nano Institute of Utah, University of Utah, Salt Lake City, UT 84112, USA.*
E-mail: solarsaravanan50@gmail.com

† Electronic supplementary information (ESI) available: Copies of $^{1}H/^{13}C$ NMR spectra for the probe and its complex, results of NMR titration, and FT-IR spectra are included. See DOI: https://doi.org/10.1039/d3sd00146f

reported by Jalal Isaad *et al.* and Liqun Chi *et al.*[32,33] Amphiphilic tripodal sensor-based turn-on fluorescent determination of Hg^{2+} was developed in an aqueous solution with relevant analytical application[34] and a ruthenium(II) polypyridine-based fluorescent sensor was developed as a luminescent probe for the detection of mercury ions.[35] Highly selective and fast visual response of the detection of mercury ions and its application in buffer-free real water samples[36] are well-documented. Application on bioimaging and paper strips with a phenothiazine probe for the detection of mercury ions[37] and lysosome-targetable fluorescent sensor with highly selective Hg^{2+} in environmental water samples and bioimaging[38] have been reported. The cyclization between phenol and acetylene to form benzofuranyl mercury chloride was discussed by Dong-Gyu Cho *et al.*[39] Keun-Hyeung Lee *et al.* reported enhanced fluorescence of a sensor based on an amino acid for Pb^{2+} and Hg^{2+} detection in an aqueous medium.[40,41] Tridentate lysine-based sensors for the detection of Hg^{2+} in aqueous solution were reported by Li-Jun Ma *et al.*[42] Shih-Sheng Sun *et al.* designed styryl dithiaazacrown containing platinum(II) terpyridine for selective colorimetric detection of Hg^{2+}.[43] Removal of Hg^{2+} ions by environmental samples and the use of[44–46] various voltammetric techniques for the detection of mercury ions has been discussed by Richard G. Compton *et al.*[47] The application of gold and silver nanoparticles attached to organic fluorophore has been discussed by Kien Wen Sun *et al.* and Bipul Sarkar and Palash Mondal.[48,49]

Herein, we designed an electron-rich protecting group, 1,3 propane dithiol, which might be scavenged by **Hg^{2+}** species to release the electron-lacking diphenyl imidazole benzaldehyde core. Therefore, thioacetal of probe **5** is converted to aldehyde compound **3**. Compound **3** shows a blue shift in UV-visible absorbance and fluorescence following intramolecular charge transfer (ICT) from the electron-donating diphenyl imidazole moiety to the electron-attracting aldehydic group with less intensity than probe **5**. As a result, in the context of a strategy of protection and removal of protection in the probe, the arrangement of electrons in the aldehydic functional group could utilize ICT to produce a large wavelength with high emission intensity, whereas the intensity of emission of probe **5** decreased upon adding **Hg^{2+}** to the aqueous medium. It was found that the fluorescence intensity of the probes increased linearly with the **Hg^{2+}** concentration over a wide range of concentrations. Thus, the intensity of emission was restored by adding **CN^-** ions to replace **Hg^{2+}**. These changes indicate the capability of sensor **5** and its **5** + **Hg^{2+}** group for measurable detection of **Hg^{2+}**, as well as the recovery of fluorescence by **CN^-** as an "on–off–on" type probe.

2. Results and discussion

2.1 Preparation of compound 3

Here, 0.643 grams of terepthaldehyde and 2.95 grams of ammonium acetate were dissolved in 30 mL of ethanol. A small amount of benzil (1 g) was added to the reaction mixture after it had been slightly warmed. The reaction mixture was heated for about 6 hours. The dark orange crude product was obtained by evaporating the solvent under vacuum. In the final step, hexane/ethyl acetate (95/5, v/v) was used as an eluent for silica gel chromatography to produce 1.31 g of the crude product (yield: 84%).

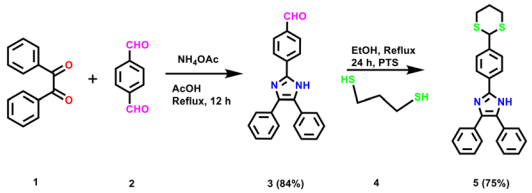

Scheme 1 A synthetic route for the synthesis of 2-(4-(1,3-dithian-2-yl)phenyl)-4,5-diphenyl-1*H*-imidazole.

2.2 Synthesis of sensor compound 5

Sensor **5** was readily synthesized from aldehyde by coupling between diphenylimidazo benzaldehyde **5** (0.5 g) and 1,3-propanedithiol (0.185 mL) catalyzed by *p*-toluenesulfonic acid using ethanol as solvent under reflux condition for 12 h. The reaction mixture was heated until the starting materials had dissolved. Further purification was achieved using column chromatography hexane/ethyl acetate (90/10, v/v) and 0.43 g of compound **5** (yield: 75%) was obtained. The structure was determined using NMR spectroscopic and HRMS techniques (ESI† Fig. S1–S3) (Scheme 1).

2.3 The absorption selectivity and titration studies of the probe

Probe **5** was evaluated for colorimetric and fluorescence emission responses to a variety of metal ions in a CH_3CN/H_2O mixture (8 : 2, v/v) as the medium. Sensor compound **5** had maximum absorption around 260–360 nm related to π–π* transitions, making the compound solution colorless. The changes in the absorption maximum with the introduction of various metal ions, including Cr^{3+}, Li^+, Cd^{2+}, Hg^{2+}, Na^+, Ni^{2+}, Pb^{2+}, Al^{3+}, Co^{2+}, Ag^+, Zn^{2+}, Sr^{2+}, Ba^{2+}, Mg^{2+}, Bi^{3+}, Th^{4+} and Fe^{3+} are described (Fig. 1). Upon the addition of 100 μL of Hg^{2+} ion, the absorption spectrum of compound **5** exhibited a marked red shift when compared to probe **3**. This red shift was attributed to ICT. In addition, the red shift in absorption indicates that, indeed, the aldehyde group acts as an electron-withdrawing group in the ICT process. To assess probe **5** as a colorimetric sensor for **Hg^{2+}**, titrations were performed with successive additions of **Hg^{2+}** (0 to 1.6 equiv.) to a solution of probe **5**. With the addition of increasing amounts of **Hg^{2+}** the absorbance at 315 nm decreased gradually while a new absorption band at 233 nm (blue shift) developed, which induced a color change from colorless to light yellow, due to the internal charge transfer (ICT) between sulfur group attached probe **5** towards **Hg^{2+}** ion. The isosbestic absorption point was observed at 220 nm upon the addition of Hg^{2+}, which indicated

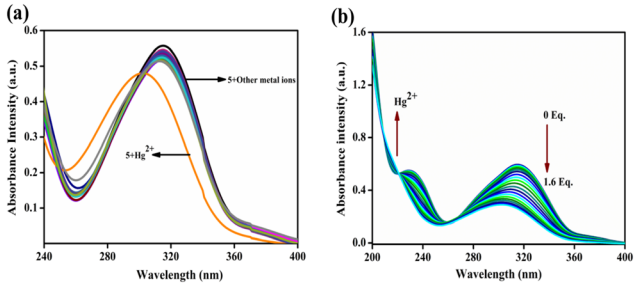

Fig. 1 (a) The UV-visible absorption spectra of sensor **5** (2 μM) upon addition of different metal cations to CH_3CN/H_2O (8 : 2, v/v) solution. (b) Titration of sensor **5** (2 μM) with increasing concentration of Hg^{2+} ion (1 mM).

a large wavelength shift in the isosbestic point with clear reproduction of compound **3**.

2.4 The fluorescence selectivity and titration studies of probe 5

The emission properties of probe **5** in the presence of different metal ions were studied in a CH_3CN/H_2O (8 : 2, v/v) system. Probe **5** displayed high emission intensity with a longer wavelength at 340–475 nm. Except Hg^{2+}, other competing metal ions, such as Cr^{3+}, Li^{+}, Cd^{2+}, Hg^{2+}, Na^{+}, Ni^{2+}, Pb^{2+}, Al^{3+}, Co^{2+}, Ag^{+}, Zn^{2+}, Sr^{2+}, Ba^{2+}, Mg^{2+}, Bi^{3+}, Th^{4+} and Fe^{3+} did not show any spectral changes. The introduction of Hg^{2+} ion resulted in quenching of an intense emission peak at 385 nm as shown in Fig. 2a. The emission titration of compound **5** with 0 to 1.6 equivalent of Hg^{2+} ion step-by-step showed quenching of the fluorescence emission at 385 nm with a linear relationship between the concentration of **Hg^{2+}** and a decrease in the intensity of fluorescence. Due to the electron-rich nature, the thioacetal group could be easily eliminated by **Hg^{2+}** to release the electron-seeking aldehydic group resulting in a strong push–pull electron system. Furthermore, the detection limit of probe **5** toward **Hg^{2+}** was measured by plotting emission intensity against the concentration of **Hg^{2+}** ion. This plot showed good linearity (ESI† Fig. S4), and a detection limit of 5.3 nM was found,

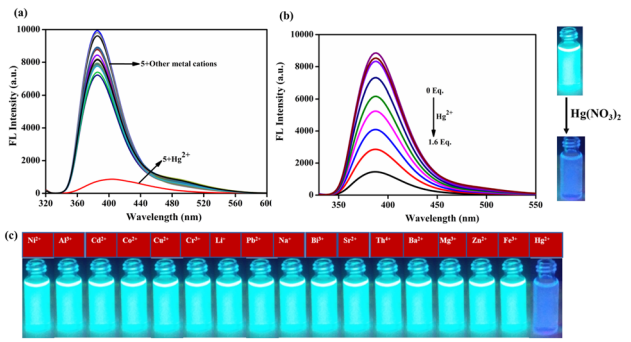

Fig. 2 (a) Sensor **5** (2 μM) fluorescence spectra with different metal ions in CH_3CN/H_2O (8 : 2, v/v) solution. (b) Compound **5** (2 μM) was treated with different equivalents of Hg^{2+} ion (1 mM, 0 to 1.6 equivalents).

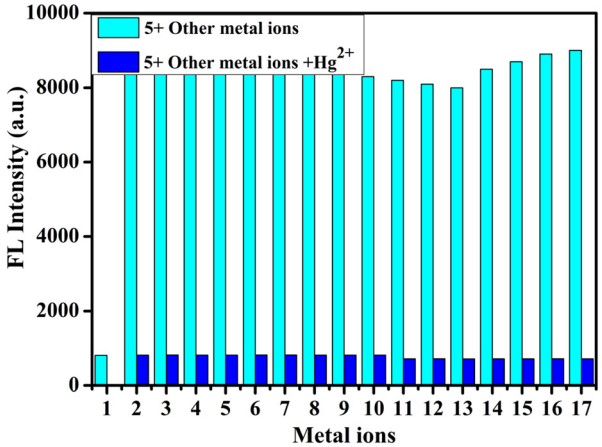

Fig. 3 Emission intensity of compound **5** in the presence of Hg^{2+} (2 equivalents cyan bars) and competitive metal ions (2 equivalents blue bars) which are shown in 1: Hg^{2+}, 2: Cr^{3+}, 3: Cd^{2+}, 4: Li^{+}, 5: Ni^{2+}, 6: Sr^{2+}, 7: Na^{+}, 8: Pb^{2+}, 9: Al^{3+}, 10: Co^{2+}, 11: Ag^{+}, 12: Zn^{2+}, 13: Ba^{2+}, 14: Mg^{2+}, 15: Fe^{3+}, 16: Th^{4+} and 17: Bi^{3+}.

which is reasonably low for the limit of detection of **Hg^{2+}** in comparison with earlier reports on sensor performance (ESI† Table S1).

2.5 Interference study

The emission experiment was conducted to study interference by different metal ions by adding two equivalents of **Hg^{2+}** ions and also two equivalents of other metal ions (Cr^{3+}, Li^{+}, Cd^{2+}, Hg^{2+}, Na^{+}, Ni^{2+}, Pb^{2+}, Al^{3+}, Co^{2+}, Ag^{+}, Zn^{2+}, Sr^{2+}, Ba^{2+}, Mg^{2+}, Bi^{3+}, Th^{4+}, and Fe^{3+}) to sensor **5** solutions. In the presence of **Hg^{2+}**, the emission intensity did not change significantly when other metals were added. Hence, it has good selectivity for Hg^{2+} ions as compared to other metal ions (Fig. 3).

2.6 pH study

We measured the emission response of probe **5** at different pH values to study the pH effect on the emission response with and without **Hg^{2+}**. The results of the experiment suggest that the emission of compound **5** was not affected in the pH range of 6–12. The fluorescence intensity of probe **5** was high and constant within a pH range of 6–12, indicating that it was not affected by pH. However, **5** with **Hg^{2+}** showed decreased fluorescence intensity at pH levels 2 to 6. Fluorescence intensity also decreased within five seconds after the addition of **Hg^{2+}** ions. These results imply that there is an instant protection/deprotection occurring with the aldehyde and thiol groups. These tentative data prove that probe **5** can be used in biological systems and that the fluorescence intensity of **5** with **Hg^{2+}** remains constant in the physiological pH range (Fig. 4).

2.7 Response time study

We studied the reaction response time between probe **5** and the **Hg^{2+}** ion using time-dependent fluorescence spectra. The

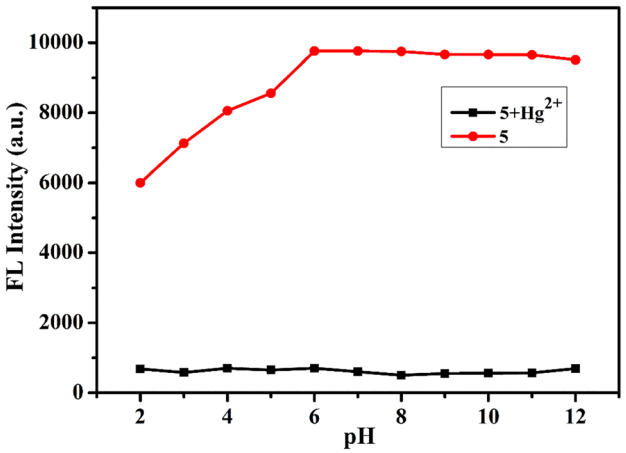

Fig. 4 Compound **5** and **5** + Hg^{2+} emission intensities at different pH levels.

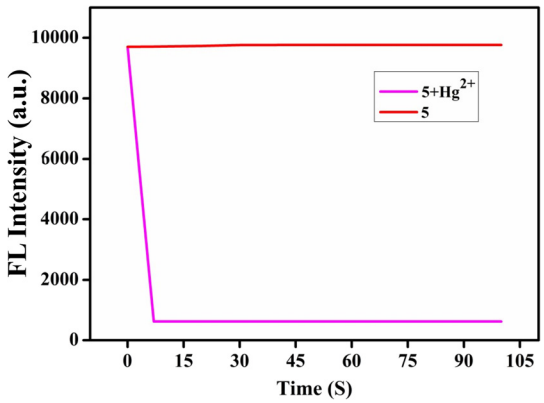

Fig. 5 Sensor **5** with Hg^{2+} ion response time.

fluorescence emission intensity of sensor **5** at 385 nm immediately decreased in the presence of Hg^{2+} ion within 15 s and remained unchanged for more than 100 s. Sensor **5** detected Hg^{2+} ions quickly (Fig. 5).

2.8 Plausible sensing mechanism

The ^{1}H NMR spectroscopic titration of probe **5** with Hg^{2+} ion in DMSO-d6 solvent further explored the interaction between probe **5** and Hg^{2+} ion. With the addition of Hg^{2+} to probe **5**, the CH proton at 5.45 ppm disappeared completely. This was followed by the formation of a new proton signal at 10.01 ppm due to the formyl group. Furthermore, the ^{1}H NMR spectra of probe **5** upon reaction with Hg^{2+} were quite similar to that of compound **3** indicating that the 1,3 propane dithiane unit in probe **5** was successfully deprotected, and the aldehyde group was formed in the presence of Hg^{2+} as described in ESI† Fig. S5. The sensing mechanism of probe **5** for Hg^{2+} was also investigated by FT-IR spectra, which is depicted in ESI† Fig. S7. On the introduction of Hg^{2+}, the new bands appeared at 1656 and 2926 cm^{-1} related to the

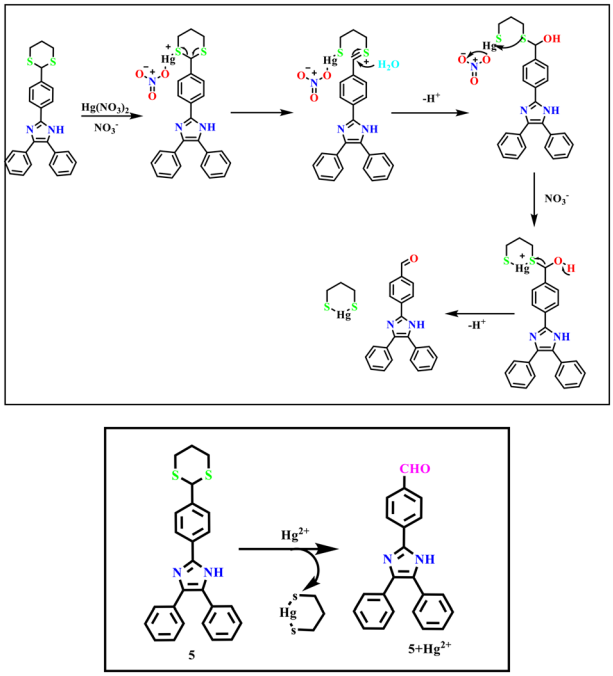

Scheme 2 Proposed mechanism for detecting Hg^{2+} by**5**.

C(H)═O and C(═O)–H groups, respectively. In line with probe **3**, this result was also obtained. Moreover, the analysis of the HRMS spectrum of the probe clearly illustrates that the molecular ion peak was found at *m*/*z* 414.1380 but was changed to *m*/*z* 324.2122 when Hg^{2+} ions were introduced (ESI† Fig. S8). This is the same as compound **3** (ESI† Fig. S10), which confirms the deprotection of thiols in the presence of Hg^{2+} ions, which frees up an aldehyde group (Scheme 2).

2.9 DFT computational calculation studies

To further investigate the proposed mechanism of probe **5** joining the Hg^{2+} ion, Gaussian 09 software was used to perform DFT calculations using the B3LYP/6-311g (d, p) method.[53,54] The optimized structure of compound **5** and **5** + Hg^{2+} are given in Fig. 6 and the corresponding details of bond lengths and bond angles are listed in ESI† Tables S2–S4. As displayed in Fig. 7, the HOMO of compound **5** was only spread over the benzene and imidazole ring, while the LUMO ranged across the entire molecule, except the 1,3 dithiane portions and the biphenyl unit. After binding of the Hg^{2+} ion, the electron density in the HOMO was distributed over the benzaldehyde part, while the entire molecule behaves as LUMO. According to the DFT calculations, the energy gap between HOMO and LUMO of **5** was 3.96 eV and that of **5** + Hg^{2+} was 3.40 eV. As a result of the conversion to the aldehyde unit, the band gap decreased by 0.56 eV. According to this observation, the energy gap decreased, and the wavelength presented a hypochromic shift, which is in agreement with the experimental results.

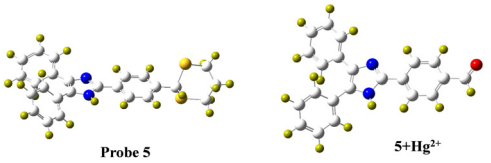

Fig. 6 Optimised structure of probe **5** and optimised structure of **5** + Hg^{2+}.

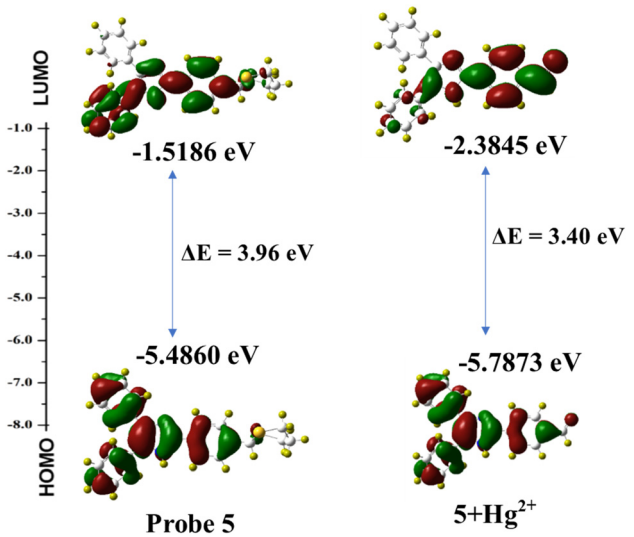

Fig. 7 HOMO and LUMO energy difference between **5** and **5** + Hg^{2+}.

2.10 Application in cell-imaging

In this study, we evaluated the ability of sensor probe **5** to detect Hg^{2+} ions in *E. coli* cells using a fluorescence microscope. Fig. 8a shows a bright field image of *E. coli* cells soaked in probe **5** for 30 minutes in an aqueous medium. In Fig. 8b, the *E. coli* cells soaked in probe **5** showed blue color fluorescence after 30 minutes of incubation. In contrast, a bright field image of *E. coli* cells incubated with probe **5**, and then in 5 μM of Hg^{2+}, followed by being kept for 10 minutes at incubation is given in Fig. 8c. Fig. 8d shows that blue color fluorescence was quenched significantly after the addition of incubated *E. coli* cells to probe **5** for 10 minutes and incubated with 5 μM of Hg^{2+} ion solution. As a result of these changes, sensor **5** can detect Hg^{2+} ions in *E. coli* cells.

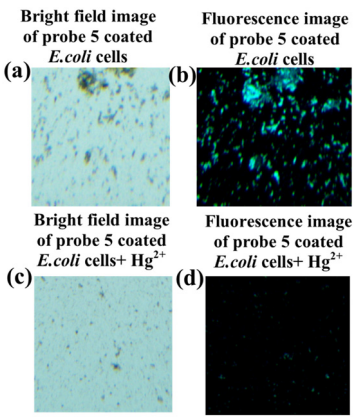

Fig. 8 Probe **5** and **5** + Hg^{2+} images taken in the visible region. (a) and (b) Images showing bright field and fluorescence of *E. coli* cells loaded with probe **5** (2 μM). Figure (c) and (d) a bright field and fluorescence image of *E. coli* cells further exposed to Hg^{2+} ion (5 μL) for 10 minutes with probe **5** (2 μM).

2.11 Real sample analysis

Sensor **5** was used to detect Hg^{2+} ions in samples of various sources of water, including distilled water, as well as water from a lake and a pond in VIT, Vellore, India. We spiked these water samples with a known amount of Hg^{2+} nitrate. These water samples were used for the analysis quantitatively. The emission intensity variations were measured by sensor **5** upon the introduction of various spiked amounts of Hg^{2+} ions. We have summarized the results of recovery, relative standard deviation (R.S.D) values (Table 1), and atomic absorption spectroscopy (AAS) using adsorption of mercury ions; a linear plot has been illustrated in ESI† Fig. S6. The emission intensities suggested that sensor **5** has a very good percentage of recovery for Hg^{2+} (95.40–102.4%). The introduction of the Hg^{2+} ion to sensor **5** in the solution form clearly showed the change in color from cyan blue to blue in the UV light. These results confirm that sensor **5** is applied to sensing the amount of Hg^{2+} ion spiked water samples with almost complete recovery, so that we can use this sensor for practical applications.

2.12 Cytotoxicity study

The MTT assay of probe **5** to HeLa cells was measured by a standard, 3-[4,5-dimethylthiazol-2-yl] 2,5-diphenyltetrazolium bromide (MTT), which is a yellow colored water-soluble salt. A mitochondrial enzyme in living cells, succinate-dehydrogenase, cleaves the tetrazolium ring, converting MTT to insoluble purple formazan. Therefore, the amount of formazan produced is directly proportional to the number of viable cells. After 48 h of incubation, 15 μL of MTT (5 mg mL^{-1}) in phosphate-buffered saline (PBS) was added to each well and incubated at 37 °C for 4 h. The medium with MTT was then flicked off and the formazan crystals formed were solubilized in 100 μL of DMSO. Absorbance was then measured at 570 nm using a microplate. The obtained results indicated that the receptors are non-toxic to the cells under experimental conditions (ESI† Fig. S9). The bright field and fluorescence images were taken through fluorescence microscopy with excitation at 365 to 450 (±10) nm. HeLa cells were incubated with probe **5** for 10 min at room temperature; they displayed yellowish-green fluorescence in the intracellular region. Upon further incubation of cells with Hg^{2+} for another 10 min, they exhibited decreasing intracellular fluorescence, indicating that the intracellular uptake of Hg^{2+} resulted in the proposed desulfurization mechanism and was confirmed by the detection of Hg^{2+} in

Table 1 The detection of Hg^{2+} ions in water samples collected from the VIT region (Vellore, TN, India) using sensor 5

Sample	Hg^{2+} added (μM)	Hg^{2+} found (μM)	Recovery (%)	R.S.D[a] (n = 3) %
Pond water	25	23.85	102.4%	0.0255
	50	50.22	101.2%	0.0243
	75	75.90	99.5%	0.0270
Lake water	25	24.89	99.6%	0.0261
	50	49.99	100%	0.0219
	75	75.80	101.1%	0.0210
Distilled water	25	25.59	95.40%	0.0204
	50	50.61	100.4%	0.0218
	75	74.59	101.20%	0.0220

[a] R.S.D. relative standard deviation; conditions: 20.00 μM of probe 5 in a mixed solution of acetonitrile/ real water (8 : 2).

the intracellular region (Fig. 9). This study result provides important aspects for the development of a new probe for Hg^{2+} detection in living cells by fluorescence imaging.

2.13 Cell imaging assay

The probe sensing system was used for *in vitro* imaging of mercury in live HeLa cells. HeLa cells were obtained from NCCS, Pune. The cells were cultured in Dulbecco's modified Eagle medium (DMEM) with 100 U mL^{-1} penicillin, 10% fetal bovine serum (FBS), and 100 mg mL^{-1} streptomycin under 5% CO_2 at 37 °C. After 24 h of incubation in DMEM, 20 μL of the probe (10 μM) was incubated with 980 μL of a cell solution in DMEM for 10 min at 37 °C, and the cells were washed thrice with PBS buffer solution (10 mM, pH 7.4). The fluorescence imaging of cells was performed on a confocal microscope. Afterward, 1.0 mL of different concentrations of Hg^{2+} solutions (5 and 10 μM) in PBS buffer (10 mM, pH 7.4) was added to the above cells for incubation for another 10 min. The cells were then washed thrice with PBS buffer solution (10 mM, pH 7.4), and fluorescence imaging of the cells was carried out. The excitation and emission wavelengths were kept at 365 nm and 450 (±10) nm, respectively.

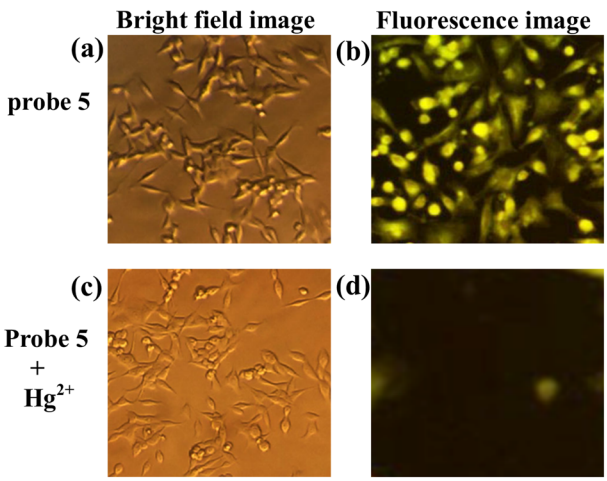

Fig. 9 Cell imaging with probe 5 and probe 5+Hg^{2+} in HeLa cells. (a) and (b) Bright field and fluorescence image of HeLa cells loaded with probe 5 (20 μM) for 10 minutes. (c) and (d) Bright field and fluorescence image of cells incubated with probe 5 (20 μM) further exposed to Hg^{2+} (10 μM) for 10 minutes.

3. Conclusion

The overall objective of this work was to design and synthesize a new probe for the detection of **Hg^{2+}** in CH_3CN : H_2O (8 : 2, v/v) solution using 2-(4-(1,3-dithian-2-yl) phenyl)-4,5-diphenyl-1*H*-imidazole as an indicator. In the presence of other metal ions, sensor 5 showed a unique colorimetric and fluorescence turn-off response, showing that it has higher selectivity than other metal ions. Fluorescence color can be observed under UV light at 365 nm with significant changes. A detection limit of 5.3 nM was calculated for compound 5. According to WHO guidelines, the LOD was well below the maximum acceptable limit in drinking water. By using ^1H NMR titration and DFT studies, the sensing mechanism of the reaction was verified. Additionally, probe 5 detected **Hg^{2+}** ions in both living cells and environmental water samples. Further, test strips were made based on compound 5, which also showed superior selectivity for **Hg^{2+}** in organic semi-aqueous solutions. Test paper strips could serve as a feasible and convenient method of detecting **Hg^{2+}** in test kits.

4. Experimental section

4.1 Reagents

Benzil, terepthaldehyde, and nitrate salts of Cr^{3+}, Li^{+}, Cd^{2+}, Hg^{2+}, Na^{+}, Ni^{2+}, Pb^{2+}, Al^{3+}, Co^{2+}, Ag^{+}, Zn^{2+}, Sr^{2+}, Ba^{2+}, Mg^{2+}, Bi^{3+}, Th^{4+}, and Fe^{3+} were purchased from Fine Chemical Houses, Sigma Aldrich, and TCI. Other materials, such as NH_4OAc, 1,3-propane dithiol, and solvents, such as C_2H_5OH, CH_3CN, *n*-hexane, and ethyl acetate, were obtained from local chemical supplier, Avra Synthesis Pvt. Ltd and were used as such without further purifications. Double distilled water was used during the spectroscopic experiments.

4.2 General methods

We recorded the melting point values of synthesized compounds with the help of the digital melting point

apparatus Deep Vision. We collected the NMR (^{1}H NMR: 400 MHz and ^{13}C NMR: 100 MHz) spectra on a Bruker NMR instrument in DMSO-d_6. Jasco-4100 IR spectrophotometer was employed to record the FT-IR spectra. With the use of a WEXWOX fluorescence microscope 3000 with ultraviolet excitation, fluorescent bioimaging experiments were conducted. Waters-Xevo G2-XS-Q ToF was employed to record the HRMS spectrum. A Shimadzu UV-1700 spectrophotometer was used to record UV-vis absorption and the Hitachi F-2500 instrument was deployed to record emission spectra.

4.3 Spectroscopic procedure

The stock solution of free sensor **5** (1 mM) was prepared in CH_3CN solvent and the solution of nitrate salts of Cr^{3+}, Li^+, Cd^{2+}, Hg^{2+}, Na^+, Ni^{2+}, Pb^{2+}, Al^{3+}, Co^{2+}, Ag^+, Zn^{2+}, Sr^{2+}, Ba^{2+}, Mg^{2+}, Bi^{3+}, Th^{4+}, and Fe^{3+} were prepared in double distilled water. The excitation wavelength was 320 nm and the excitation slit widths were 5 nm.

4.4 Limit of detection

The limit of detection (LOD)[50] was found using the following expression based on the literature:

$$\mathrm{LOD} = 3\sigma/s.$$

Therein, σ = standard deviation of the sensor for blank measurements (n = 10), s = slope value obtained from the linear plot (fluorescence intensity of **5** *versus* the amount of Hg^{2+}).

4.5 Quantum yield

The emission quantum yield of sensor **5** with and without the introduction of Hg^{2+} ion was calculated by comparison with quinine sulfate[51] as the standard reference in sulfuric acid as per the following equation:

$$\phi_u = \phi_s X A_S X F_U X n^2 / A_U X F_S X n_0{}^2$$

Where ϕ_u and ϕ_s are quantum yields for the sample and reference, F_U and F_S are the integrated areas under the corrected fluorescence spectra for the sample and reference; A_U and A_S are the absorbance for the sample and reference, n and n_0 are the refractive indexes of the solvents used for samples and reference. The quantum yield of probe **5** was 1.01. After the addition of the Hg^{2+} ion, the quantum yield decreased to 0.293.

4.6 Synthesis of 4-(4,5-diphenyl-1*H*-imidazol-2-yl) benzaldehyde (3)

Benzaldehyde (**3**) was prepared by a previously reported procedure.[52] ^{1}H NMR [400 MHz, DMSO-d_6]: 7.25 (d, 2H, J = 5.2 Hz, ArCH), 7.33 (s, 2H, ArCH), 7.41 (d, 2H, J = 5.6 Hz, ArCH), 7.47 (s, 2H, ArCH), 7.53 (d, 2H, J = 9.6 Hz, ArCH), 8.01 (d, 2H, J = 8 Hz, ArCH), 8.30 (d, 2H, J = 8.8 Hz, ArCH), 10.03 (s, 1H, CHO), 13.02 (s, 1H, NH); ^{13}C NMR[100 MHz, DMSO-d_6]: 125.8 (2 × ArCH), 127.2 (2 × ArCH), 127.5 (2 × ArCH), 128.7 (2 × ArCH), 129.0 (4 × ArCH), 129.1 (2 × ArC), 130.0 (2 × ArCH), 130.5 (ArC), 135.8 (2 × ArC), 135.9 (ArC), 144.6 (ArC), 192.9 (ArCHO). GCMS for $C_{22}H_{16}N_2O$ calculated m/z: $[M]^+$ 324.3830; found: 324.4087 (ESI† Fig. S3).

4.7 Synthesis of 2-(4-(1,3-dithian-2-yl)phenyl)-4,5-diphenyl-1*H*-imidazole (5)

A mixture of diphenylimidazobenzaldehyde **3** (0.5 g, 1.0 equiv.) and 1,3-propane dithiol **4** (0.121 mL, 1.2 equivalent) were refluxed at 90 °C in ethanol solvent for 12 h. After cooling, the solvent was removed from the vacuum. The resultant residue was purified by column chromatography using hexane/ethyl acetate (90 : 10, v/v) to afford compound **5** as a white solid (0.58 g). Yield: 65%; melting point: 238–240 °C. FT-IR (cm^{-1}): 3061.03, 2904.80, 1695.43, 1604.77, 1487.12, 1442.75, 1413.82, 1323.17, 1274.95, 1207.44, 1170.79, 1126.43, 1068.56, 970.19, 912.33, 850.61, 831.32, 765.74, 734.88, 694.37, 673.16, 603.72, 513.07, and 422.41. ^{1}H NMR [400 MHz, DMSO-d_6]: 1.704 (m, 2H, J = 2.8 Hz, CH_2), 2.138 (m, 2H, J = 2 Hz, CH_2), 2.894 (m, 2H, J = 3.6 Hz, CH_2), 5.457 (s, 1H, J = 6.4 Hz, CH), 7.274 (t, 2H, J = 8 Hz, CH), 7.331 (t, 1H, J = 14.8 Hz, CH), 7.403 (t, 2H, J = 12.4 Hz, CH), 7.472 (m, 7H, J = 12.8 Hz, CH), 8.059 (d, 2H, J = 8.4 Hz, CH), 12.719 (s, 1H, NH); ^{13}C NMR [100 MHz, DMSO-d_6]: 25.24 (CH_2), 31.49 (2 × CH_2), 50.23 (CH), 125.95 (2 × ArCH), 127.02 (2 × ArCH), 127.54 (2 × Ar–CH), 128.29 (ArCH), 128.42 (ArCH), 128.66 (2 × ArCH), 128.90 (2 × ArCH), 129.13 (2 × Ar–CH), 130.73 (2 × Ar–CH), 135.56 (ArC), 137.70 (2 × ArC), 139.84 (C), 145.51 (ArC). HRMS (ESI/TOF-Q) for $C_{25}H_{22}N_2S_2$ calculated $[M^+]$ m/z was 414.1224, found: 414.1280.

Conflicts of interest

The authors report no declarations of interest.

Acknowledgements

Uma Krishnan is deeply grateful for the financial support she has received from VIT in the form of a Research Associateship. It is important to acknowledge the contribution of VIT-SIF and IIT Madras to the characterization studies. For language polishing, the authors thank Dr. R. Srinivasan, VIT-SSL.

Notes and references

1 W. Lin, L. Yuan, W. Tan, J. Feng and L. Long, *Chem. – Eur. J.*, 2009, **15**, 1030–1035.
2 Y. Guo, J. An, H. Tang, M. Peng and F. Suzenet, *Mater. Res. Bull.*, 2015, **63**, 155–163.
3 E. Bozkurt and H. I. Gul, *Sens. Actuators, B*, 2018, **255**, 814–825.

4 K. M. Vengaian, C. D. Britto, K. Sekar, G. Sivaraman and S. Singaravadivel, *Sens. Actuators, B*, 2016, **235**, 232–240.
5 Z. Wang, Y. Zhang, J. Yin, Y. Yang, H. Luo, J. Song, X. Xu and S. Wang, *ACS Sustainable Chem. Eng.*, 2020, **8**, 12348–12359.
6 A. Chatterjee, M. Banerjee, D. G. Khandare, R. U. Gawas, S. C. Mascarenhas, A. Ganguly, R. Gupta and H. Joshi, *Anal. Chem.*, 2017, **89**, 12698–12704.
7 X. Xu, Y.-F. Li, J. Zhao, Y. Li, J. Lin, B. Li, Y. Gao and C. Chen, *Analyst*, 2015, **140**, 7841–7853.
8 A. Singh, S. Kaur, N. Singh and N. Kaur, *Org. Biomol. Chem.*, 2014, **12**, 2302–2309.
9 J. Hu, J. Li, J. Qi and J. Chen, *New J. Chem.*, 2015, **39**, 843–848.
10 S. K. Patil and D. Das, *Spectrochim. Acta, Part A*, 2019, **210**, 44–51.
11 P. Cas, J. Shanmugapriya, S. Singaravadivel, G. Sivaraman and D. Chellappa, *ACS Omega*, 2018, **3**, 12341–12348.
12 U. Krishnan and S. K. Iyer, *J. Photochem. Photobiol., A*, 2022, **425**, 113663.
13 C. Parthiban, R. Manivannan and K. P. Elango, *Dalton Trans.*, 2015, **44**, 3259–3264.
14 S. Lei, X. Meng, L. Wang, J. Zhou, D. Qin and H. Duan, *ChemistryOpen*, 2021, **10**, 1116–1122.
15 A. Picard-Lafond, D. Larivière and D. Boudreau, *ACS Omega*, 2019, **5**, 701–711.
16 J. Orrego-Hernández, J. Cobo and J. Portilla, *ACS Omega*, 2019, **4**, 16689–16700.
17 J. Pan, J. Ma, L. Liu, D. Li, Y. Huo and H. Liu, *J. Photochem. Photobiol., A*, 2021, **416**, 113322.
18 Y. Li, W. Shi, J. Ma, X. Wang, X. Kong, Y. Zhang, L. Feng, Y. Hui and Z. Xie, *J. Photochem. Photobiol., A*, 2017, **338**, 1–7.
19 Y. Yang, Y. Feng, Y.-Z. Wang, F.-Z. Qiu, X.-L. Tang, G.-L. Zhang and W.-S. Liu, *Sens. Actuators, B*, 2017, **253**, 1055–1062.
20 Z. Ma, D. Zhang, J. Guo, M. Li, T. Wang, H. Yin, H. Wang and J. Liu, *Inorg. Chem. Commun.*, 2021, **130**, 108753.
21 E. M. Nolan, M. E. Racine and S. J. Lippard, *Inorg. Chem.*, 2006, **45**, 2742–2749.
22 A. Pariyar, S. Bose, S. S. Chhetri, A. N. Biswas and P. Bandyopadhyay, *Dalton Trans.*, 2012, **41**, 3826–3831.
23 Y. Zhao, Z. Lin, C. He, H. Wu and C. Duan, *Inorg. Chem.*, 2006, **45**, 10013–10015.
24 S.-M. Cheung and W.-H. Chan, *Tetrahedron*, 2006, **62**, 8379–8383.
25 V. Tekuri, S. K. Sahoo and D. R. Trivedi, *Spectrochim. Acta, Part A*, 2019, **218**, 19–26.
26 T. G. Akshay Krishna, V. Tekuri, M. Mohan and D. R. Trivedi, *Sens. Actuators, B*, 2019, **284**, 271–280.
27 R. R. Koner, S. Sinha, S. Kumar, C. K. Nandi and S. Ghosh, *Tetrahedron Lett.*, 2012, **53**, 2302–2307.
28 L. Lu, X. Han, J. Lin, Y. Zhang, M. Qiu, Y. Chen, M. Li and D. Tang, *Analyst*, 2021, **146**, 2664–2669.
29 M. Xu, Z. Gao, Q. Wei, G. Chen and D. Tang, *Biosens. Bioelectron.*, 2016, **79**, 411–415.
30 Z. Qiu, J. Shu, G. Jin, M. Xu, Q. Wei, G. Chen and D. Tang, *Biosens. Bioelectron.*, 2016, **77**, 681–686.
31 Z. Qiu, D. Tang, J. Shu, G. Chen and D. Tang, *Biosens. Bioelectron.*, 2016, **75**, 108–115.
32 L. Huang, W. Sheng, L. Wang, X. Meng, H. Duan and L. Chi, *RSC Adv.*, 2021, **11**, 23597–23606.
33 J. Isaad and A. El Achari, *J. Lumin.*, 2022, **243**, 118668.
34 S. De and G. Das, *Dyes Pigm.*, 2021, **195**, 109659.
35 J. Xu, Y. Liu and M.-J. Li, *Spectrochim. Acta, Part A*, 2019, **219**, 141–146.
36 X. Li, D. Xiu, J. Shi, J. Miao, Y. Yu, H. Song, J. Lin, Q. Feng and H. Yu, *Spectrochim. Acta, Part A*, 2022, **265**, 120367.
37 J. Wang, Q. Niu, T. Hu, T. Li and T. Wei, *J. Photochem. Photobiol., A*, 2019, **384**, 112036.
38 A. Sarkar, S. Chakraborty, S. Lohar, E. Ahmmed, N. C. Saha, S. K. Mandal, K. Dhara and P. Chattopadhyay, *Chem. Res. Toxicol.*, 2019, **32**, 1144–1150.
39 A. K. Atta, S.-B. Kim, J. Heo and D.-G. Cho, *Org. Lett.*, 2013, **15**, 1072–1075.
40 L. N. Neupane, J.-Y. Park, J. H. Park and K.-H. Lee, *Org. Lett.*, 2013, **15**, 254–257.
41 M.-H. Yang, P. Thirupathi and K.-H. Lee, *Org. Lett.*, 2011, **13**, 5028–5031.
42 L. Chen, L. Yang, H. Li, Y. Gao, D. Deng, Y. Wu and L.-j. Ma, *Inorg. Chem.*, 2011, **50**, 10028–10032.
43 S.-K. Chung, Y.-R. Tseng, C.-Y. Chen and S.-S. Sun, *Inorg. Chem.*, 2011, **50**, 2711–2713.
44 A. Panda, Y. Yang, S. Venkateswarlu, Y. Son, T.-H. Bae and M. Yoon, *Microporous Mesoporous Mater.*, 2020, **306**, 110399.
45 M. Shellaiah and K.-W. Sun, *Chemosensors*, 2021, **9**, 101.
46 D. Dai, J. Yang, Y. Wang and Y. W. Yang, *Adv. Funct. Mater.*, 2021, **31**, 2006168.
47 A. L. Suherman, E. E. Tanner and R. G. Compton, *TrAC, Trends Anal. Chem.*, 2017, **94**, 161–172.
48 M. Shellaiah, T. Simon, P. Venkatesan, K. W. Sun, F.-H. Ko and S.-P. Wu, *Appl. Surf. Sci.*, 2019, **465**, 340–350.
49 B. Sarkar and P. Mondal, *J. Water Environ. Nanotechnol.*, 2021, **6**, 22–40.
50 N. Kaur, G. Dhaka and J. Singh, *New J. Chem.*, 2015, **39**, 6125–6129.
51 H. A. Benesi and J. Hildebrand, *J. Am. Chem. Soc.*, 1949, **71**, 2703–2707.
52 J. Hao, L. Ruhlmann, Y. Zhu, Q. Li and Y. Wei, *Inorg. Chem.*, 2007, **46**, 4960–4967.
53 C. Adamo and D. Jacquemin, *Chem. Soc. Rev.*, 2013, **42**, 845–856.
54 P. Wen, Z. Gao, R. Zhang, A. Li, F. Zhang, J. Li, J. Xie, Y. Wu, M. Wu and K. Guo, *J. Mater. Chem. C*, 2017, **5**, 6136–6143.